10689 Session 2022
B1
PS1: LEARNING FROM EXPERIENCES

Development of Analytical Method for Power Cable Creepage Phenomenon in Duct

Tomonori KAMIBAYASHI* **Tadanori NAGAYAMA**
Tohoku Electric Power Network Co., Inc.
Katsumi IWAMURA, **Koki KASHIRO**
Furukawa Electric Co., Ltd.
Hiroyasu NISHIKUBO
FITEC Corp.
Japan
kamibayashi.tomonori.hc@tohoku-epco.co.jp nagayama.tadanori.ef@tohoku-epco.co.jp
katsumi.ki.iwamura@furukawaelectric.com koki.kk.kashiro@furukawaelectric.com
hiroyasu.nishikubo@furukawaelectric.com

SUMMARY
In Japan, most underground cables are laid in ducts buried under roads. Cable joint boxes are located at access ports where utility staff members can reach them for maintenance. In such facilities, which are under conditions of soft ground and shallow burial depth of the duct and heavy traffic, cables in the ducts might move in the direction of car motion because of cable creepage. If this phenomenon progresses excessively, especially near a joint at which the cable is fixed, stress might be concentrated in the cable, leading to severe damage. The usual countermeasure for this phenomenon is to restrain the cable in the access port. Therefore, the moving force of the cable generated by this phenomenon must be understood accurately. Research efforts elucidating the causes of this phenomenon have been dominated by the assumption that the duct deflection vertical component plays an important role. Actually, various prediction models have been proposed under the assumption, but they might differ from reality depending on the facility conditions.
This report describes that this phenomenon results from the horizontal (longitudinal) component of duct deflection caused by the car load, which deflects the buried duct locally. This deflection has a longitudinal displacement component. As the car moves, the localized duct deflection also moves in the direction of the car motion, thereby causing localized horizontal (longitudinal) motion in the duct. This localized longitudinal velocity has two components: one in the direction of the car motion (forward) and the other in the opposite direction (backward). The local longitudinal velocities in the duct cause sliding velocities between the duct and the cable. Consequently, the cable is subjected to local dynamic frictional forces. Applying the Amonton–Coulomb friction law, which states that the dynamic friction force is independent of the sliding speed, the absolute values of the dynamic friction forces are the same. The area length is greater in the forward than in the backward direction. This difference in the amounts of dynamic friction force causes the cable to move in the forward direction. Based on this theory, we have developed an analytical system that can analyze the cable creepage phenomenon. After a full-scale experiment was conducted, results of the experiment and the theoretical analysis were found to have good agreement. Furthermore, conditions for the cable creepage phenomenon to occur were discussed using this analytical system.

KEYWORDS
Amonton–Coulomb friction law, analysis system, cable creepage, power cable

1. INTRODUCTION

Fig. 1 presents an overview of typical underground cable installations in Japan. The cables are laid in ducts buried under roadways. The cable joints are located in access ports where the utility staff members can access them for maintenance. Under conditions of soft ground and shallow burial depth of the duct, cable creepage can occur: cable movement in the direction of car motion. The usual countermeasure to mitigate this phenomenon is to restrain the cable in access ports. Therefore, calculation of the cable movement force generated by this phenomenon must be done accurately. The cable movement force is often predicted using an approximate formula derived from experimentally obtained results [1], but the calculated value might differ from the actual value depending on the facility conditions.

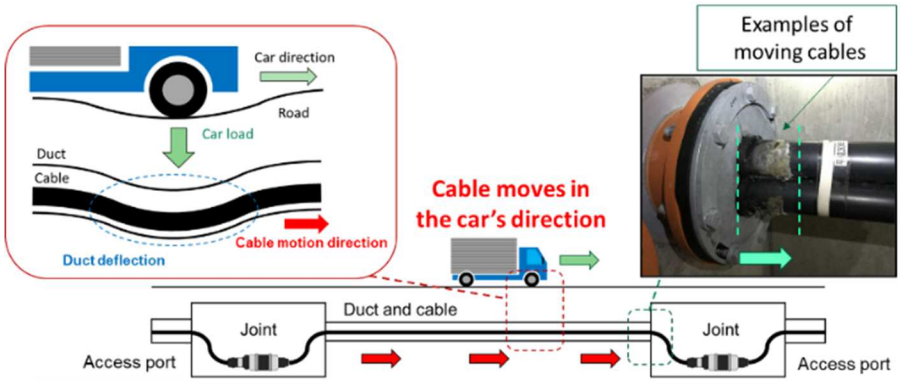

Fig. 1. Schematic diagram of cable creepage behavior.

From results of a very early study of the causes of cable creepage, Timmis [2] reported the Surf-riding theory in 1937, explaining that the duct vertical deflection is unequal in front of and behind the wheels of a passing car, and that the contact length with the cable is longer behind. Therefore, the horizontal component of the thrust tends to push the cable forward somewhat as a surf-rider advances by sliding down the wave face. However, no reason for the unequal duct deflection was explained in the report. Reportedly, the calculated cable elongation is much less than the actual measured value based on the Surf-riding theory [3]. In 1999, Kim et al. [4] reported the cable creepage causes as follows. The local horizontal (longitudinal) velocity of the duct appears in the direction of car motion (forward) and in the opposite direction (backward). The duct and cable frictional forces mutually interact. The vertical sinking of the duct caused by the car load is greater in the backward direction than in the forward direction, which decreases the contact pressure with the cable in the backward area because of the lateral elasticity of the cable. Because of this difference in contact pressure, the magnitude of the frictional force is greater in the forward direction than in the backward direction, causing the cable to move in the forward direction. Finite element method (FEM) analysis of the contact pressure between the duct and the cable in the backward area described in [4] was performed under Japanese facility conditions. Results showed that the pressure was not markedly reduced. Under Japanese equipment conditions, the decrease in contact pressure is not regarded as a major factor affecting cable creepage. Therefore, we reconsidered the mechanism of cable creepage behavior. Similarly to the method described in the report by Kim [4], the authors considered that two localized longitudinal velocity areas which appear in the duct when a car passes play important roles. Moreover, the authors considered the cause of the driving force of cable creepage behavior as different. The report presented by Kim [4] described the driving force caused by the difference of the vertical sinking between the two areas. By contrast, we considered that cable movement in the direction of car motion is caused by the dynamic frictional force caused by the relative (sliding) velocity of the cable and the duct, based on the Amonton–Coulomb friction law [5]. This law states that the dynamic friction force is independent of the sliding speed. Applying this law to the two areas of sliding velocity described above indicates the magnitude of the dynamic friction acting on the cable as the same. The action area length is greater in the forward area than in the backward area. Therefore, we conclude that the cable moves in the forward direction because the amount of dynamic friction force acting in the forward direction is greater than that in the backward direction.

Using our proposed theory based on the Amonton–Coulomb law of friction, we have developed a cable creepage analysis system that can be used easily on an ordinary PC for cable design and maintenance.

Then, full-scale experiments were conducted. The validity of this theory was confirmed by comparing experimentally obtained and analytically obtained values [6]. Furthermore, conditions of cable creepage occurrence were discussed using the analysis system developed for this study.

2. CABLE CREEPAGE PHENOMENON THEORY AND ANALYSIS SYSTEM DEVELOPMENT

2.1 Analysis of ground and duct displacement

Displacement that occurs in the ground when a car load is applied to the ground surface was analyzed using FEM software: a general-purpose nonlinear structural analysis solver. The full-scale experiment conditions described in Chapter 3 were used as analytical conditions. Fig. 2 presents the analysis conditions. The ground was composed of three layers. Each layer was treated as an elastic body with different Young's modulus and Poisson's ratio. Although the duct is shown to be at 1.2 m depth in Fig. 2, it is not modeled in the FEM analysis, assuming that the duct displaces with the ground. The car load was assumed to be a concentrated load of 20 tf, moving 1.2 m above the duct in the longitudinal direction from -4.8 m (load position A) to 4.8 m (load position E). The analysis point for ground displacement was set below load position C. Fig. 3 presents results of FEM analysis of ground displacement at the analysis points in Fig. 2. As the car load position changes from A to B to C to D to E, the ground at the analysis point is displaced vertically and longitudinally. The maximum longitudinal displacement is 16 μm. The maximum vertical displacement is 90 μm. For a homogeneous semi-infinite elastic body, the displacement inside the elastic body under the condition of a concentrated load applied to the surface was calculated using the Boussinesq equation [7]. The results resemble those obtained from this FEM analysis.

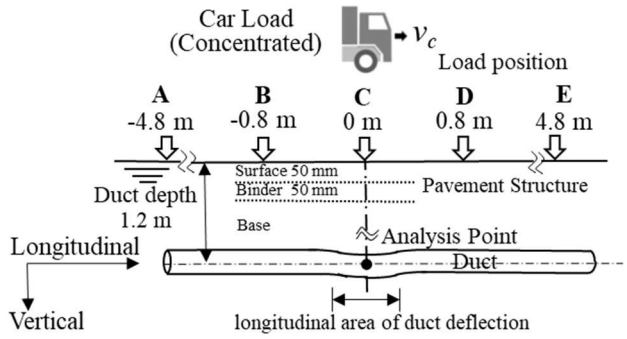

Fig. 2. Analytical conditions for ground displacement.

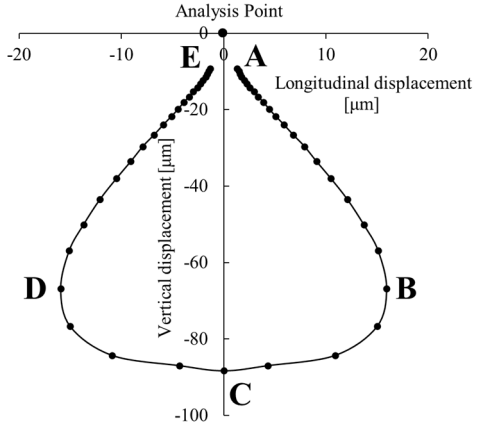

Fig. 3. Ground displacement for each car load position (FEM analysis).

Figs. 4 and 5 respectively present the vertical and horizontal (longitudinal) components of the ground displacement depicted in Fig. 3. The horizontal axis (x-axis) of these figures shows the longitudinal position of the duct, with the direction of car motion as the increasing direction of the x-axis, and with the car load acting on the origin (Fig. 2, load position C). The vertical component of the displacement presented in Fig. 4 is sinking around the load position. The longitudinal component of displacement shown in Fig. 5 is radial around the load position. The displacement changes steeply near the load position. Also the displacement decreases slowly as the car load influence decreases with distance from the load position. Solid lines in both figures present results of FEM analysis, dashed lines represent results of a two-dimensional axisymmetric FEM analysis run on an ordinary PC, as explained in section 2.4. Two lines show good agreement. When the car moves at velocity v_c in the x direction, the ground deflection moves at the same velocity. When the longitudinal displacement distribution in Fig. 5 is represented as $L(x)$, the propagation of this distribution $L(x)$ in the x-axis direction at time t is represented as $L(x\text{-}v_ct)$. After differentiating $L(x\text{-}v_ct)$ with respect to t, the longitudinal ground velocity V_l is represented by equation (1).

$$V_l(x - v_c t) = \frac{\partial L(x - v_c t)}{\partial t} = -v_c \frac{\partial L(x - v_c t)}{\partial x} \quad \cdots(1)$$

Fig. 6 shows the x-axis distribution of V_l according to equation (1) when the car passes load position C (x=0) at the velocity of v_c=40 km/h. Areas in which V_l is positive (the same direction as car motion (forward)) and negative (the opposite direction to car motion (backward)) appear. Because the products of the magnitude of the velocity and the length of these two areas are equal to those depicted in Fig. 6, the longitudinal displacement of the duct returns to its original position after the car passes.

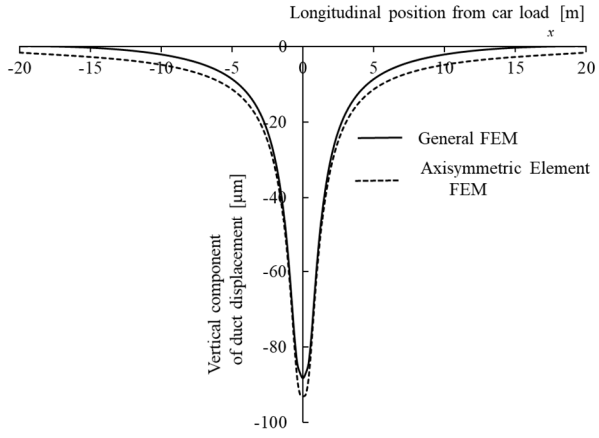

Fig. 4. Longitudinal distribution of the vertical component of ground (duct) displacement.

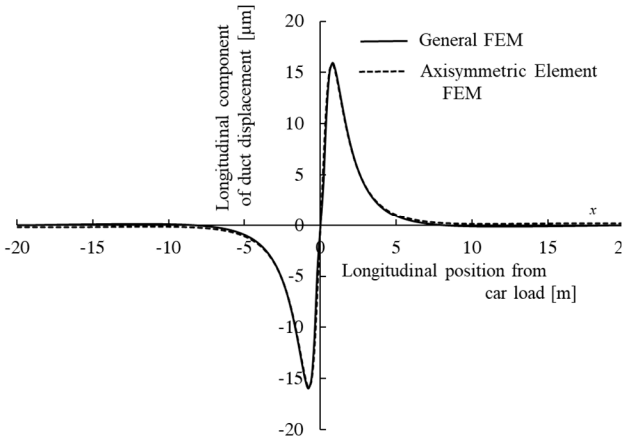

Fig. 5. Longitudinal distribution of the longitudinal component of ground (duct) displacement.

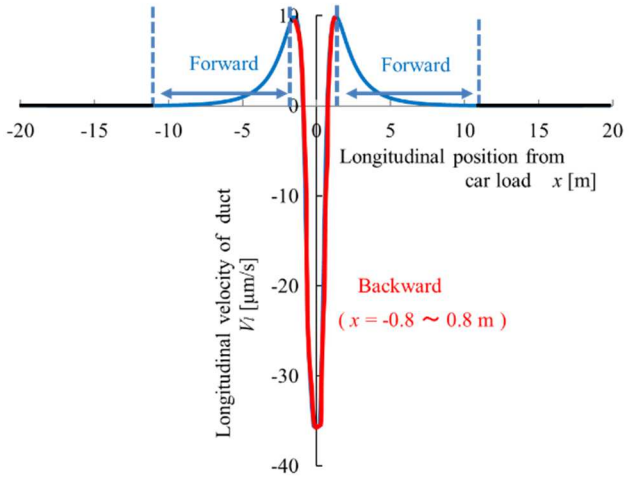

Absolute value of the longitudinal velocity
(Forward) < (Backward)
Area length of longitudinal velocity
(Forward) > (Backward)
(Absolute value) × (Longitudinal area length)
(Forward) − (Backward) = 0

Fig. 6. Longitudinal distribution of longitudinal velocity V_l of the ground (duct).

2.2 Frictional force acting on the cable and longitudinal elastic displacement

When the duct has the longitudinal displacements and velocities shown in Fig. 5 and 6, static and dynamic frictional forces act on the cables inside. Because these are localized with respect to the overall length of the cable, as portrayed in Fig. 7, the cable is discretized at regular length ΔL intervals and is modeled as a coupled lattice of mass m and longitudinal elasticity k.

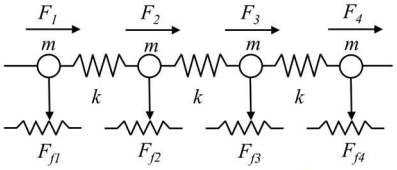

$$F_f = -\left(\frac{2}{1+e^{b\left(V_l \Delta t - u(t)\right)}} - 1\right)\mu_d mg \cdots (2)$$

Fig. 7. Discrete element model for cable analysis.

In that equation, m represents the mass of the cable element (mass point) [N], F_f stands for the dynamic frictional force acting on the mass point [N], g denotes gravitational acceleration [m/s^2], μ_d is the dynamic friction coefficient, Δt denotes the micro time interval [s], V_l expresses the relative velocity of the duct and mass point [m/s], $u(t)$ signifies the displacement of the mass point during Δt, and b is a shape factor

With the longitudinal displacement of the duct in Fig. 5, the cable is displaced elastically by the static friction force. If this amount of elastic displacement of the cable is smaller than the duct longitudinal displacement, then displacement difference occurs between the duct and cable. As the car moves longitudinally over the duct, the displacement difference also moves at the same speed. Local longitudinal sliding velocities are generated between the duct and cable. These sliding velocities consist of a forward area in the direction of the car's motion and a backward area in the opposite direction.
Based on the Amonton–Coulomb law of friction, the dynamic friction force is regarded as a constant value that is independent of the sliding speed. The dynamic friction force F_f for each divided element of the cable is calculated using equation (2). Equation (2) is a sigmoidal function that can simulate the characteristics of the dynamic friction force described above. It can stabilize the numerical calculation because it is a differentiable function. Shape factor a is a constant that incorporates the cable sheath shear deformation. [8]. Although the cable has a velocity when F_f is given at each mass point, the longitudinal distribution of the dynamic friction force calculated by equation (2) is shown in Fig. 8, approximating Fig. 6 as the sliding velocity between the cable and the duct.
In Fig. 8, x = -10 m to -0.8 m and x = 0.8 m to 10 m are forward areas at which the dynamic friction force acts in the direction of the car motion. The value of x = -0.8 m to 0.8 m is a backward area where it acts in the opposite direction. Comparison of both areas shows that the absolute values of the dynamic friction force are equal and that the length of the areas is greater in the forward area. Therefore, the product of the magnitude of the dynamic friction force and the area length is greater in the forward area direction than in the backward direction. Because of the difference in the amounts of frictional forces, the cable moves in the forward direction.

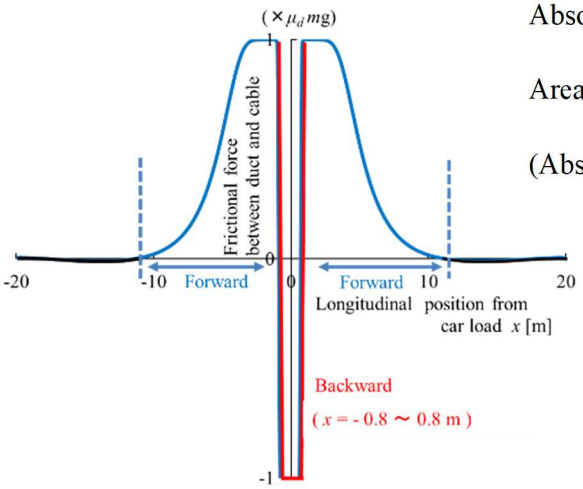

Absolute value of maximum dynamic frictional force
(Forward) = (Backward)
Area length of dynamic frictional force
(Forward) > (Backward)
(Absolute value) × (Area length)
(Forward) − (Backward) > 0

Fig. 8. Longitudinal distribution of dynamic frictional force between duct and cable.

Effects of static and dynamic frictional forces are explained further in Figs. 9 and 10. Fig. 9 panels portray schematic views of the frictional force acting on the cable in the duct. The dotted lines show displacement of the cable and duct. Fig. 10 presents formulas for the internal stress and the elastic displacement of the cable under the condition that the frictional force acts equally on the cable length X. The elastic displacement of cable is inversely proportional to the cable longitudinal elastic EA and is proportional to the square of the action length of the static frictional force on the cable. The solid line shows the displacement difference between the duct and the cable ($\Delta D_l - \Delta C_l$) under conditions in which the elastic displacement of the cable ΔC_l is smaller than the longitudinal displacement of the duct ΔD_l. As this displacement difference propagates in the x direction as the car velocity v_c, a sliding velocity is generated between them. A dynamic friction force $F_d(x\text{-}v_c t)$ acts on the cable. The dynamic friction force shown in Fig. 8 appears in the forward and backward directions, with equal absolute values and greater length in the forward direction, as shown in the schematic in the lower panel of Fig. 9. When the dynamic friction force $F_d(x\text{-}v_c t)$ finishes passing through the cable ΔX section, the duct returns to its original position, whereas the cable is displaced from the duct in the forward direction. As explained in Section 4.3, this elastic elongation of the cable is maintained and accumulated by the static frictional force between with the duct, thereby producing the cable creep phenomenon.

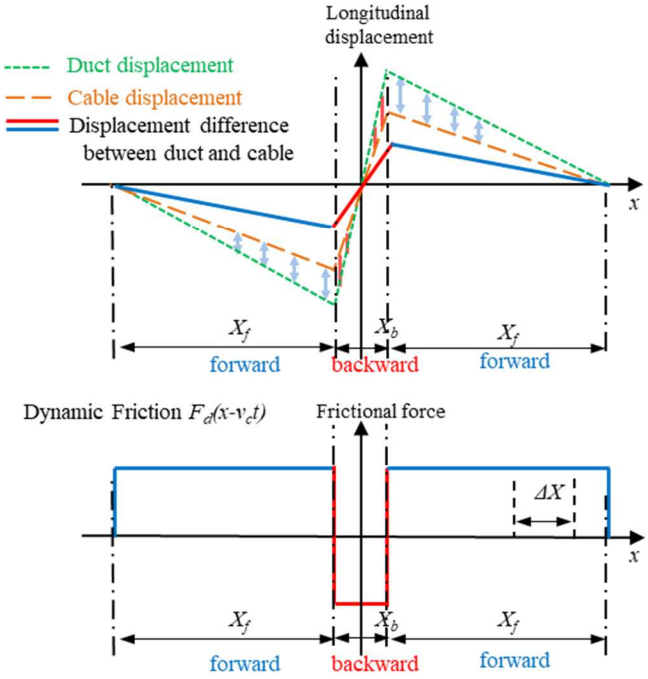

Fig. 9. Schematic diagram of frictional force acting on the cable.

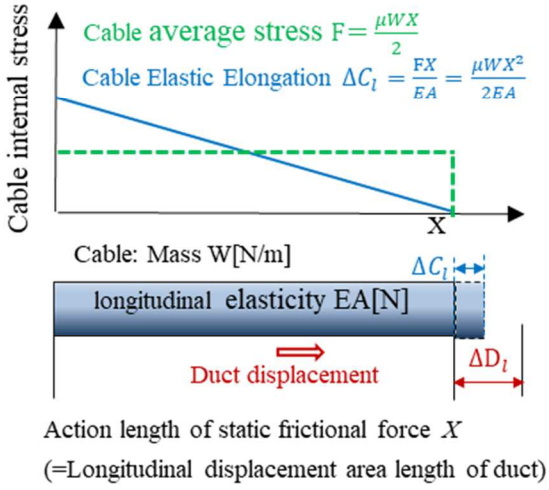

Fig. 10. Elastic displacement of cable when static friction force is applied.

2.3 Analysis of the cable

Dynamic friction force F_f is applied to each mass point portrayed in Fig. 7. From the equilibrium conditions of the cable elastic force and inertia force in Equation (3), we calculated the creepage force of the cable (internal stress of the cable) F and the displacement of the mass point (elastic expansion and contraction of cable) U. This calculation is repeated at short time intervals.

$$[k]\,\vec{U}+[m]\,\vec{a}=\vec{F}+\overrightarrow{F_f} \qquad \cdots(3)$$

Therein, $\vec{F}$ denotes the cable creepage force vector (cable internal stress) [N], $\vec{U}$ stands for displacement of a mass point vector (elastic expansion and contraction of cable) [m], $\vec{a}$ signifies the acceleration of mass points vector [m/s^2], $[k]$ is the Stiffness matrix, $[m]$ represents the cable mass matrix [N], and $\overrightarrow{F_f}$ denotes the frictional force vector between the duct and cable [N]

2.4 Development of the cable creepage analysis system

For ease of use in cable design and maintenance, we developed a cable creepage analysis system that can be run on an ordinary PC. Ground displacement was analyzed using axisymmetric element FEM in a cylindrical coordinate system with the central axis perpendicular to the road. By approximating the car as a concentrated load and approximating the duct as displaced with the ground, the analysis dimensions are reduced to two dimensions that do not change circumferentially in the cylindrical coordinate system, which greatly reduced the calculation time. The ground is treated as an elastic body. Five layers of elastic properties can be set to approximate the standard road structure in Japan. The cable was analyzed using one-dimensional discrete element method in the longitudinal direction, as portrayed in Fig. 7. The boundary conditions at the cable ends are constrained or released. In addition, a spring-loaded constraint condition can be used to elucidate countermeasures against cable creepage. Thermal expansion and contraction of the cable caused by temperature change are not considered.

3. FULL-SCALE EXPERIMENT

3.1 Overview of the full-scale experiment

A full-scale experiment was conducted, with results compared to analytical values to verify the validity of the cable creepage theory. The experiment conditions are presented in Fig. 9 and Table I. The cable (duct) length is 30 m, which is about one-tenth of the actual equipment. Polyester concrete fiberglass

reinforced plastic pipes (PFP) were used for the ducts. Two ducts were laid at 1.2 m depth. In one duct, single-core cables were laid in a trefoil formation. In the other duct, six acceleration sensors were installed at every 1 m of the duct to measure the vertical acceleration of the duct. From results of this study, we conclude that cable creepage results from longitudinal displacement of the duct, but the vertical displacement of the duct was measured for this experiment because the vertical displacement is about six times greater than the longitudinal displacement, which facilitates accurate measurement. The ground surface was covered with simple pavement. A 20 tf truck was driven repeatedly from one direction at speeds of 20, 30, and 40 km/h. The cable end of the entry side of the truck (upstream end) was set to the release condition. At the cable end of the exit side of the truck (downstream end), the compressive force of each cable was measured using load cells. Vertical deflection of the duct was calculated as 90–140 μm by integrating the measured acceleration data twice. The longitudinal area length of the duct deflection was 7–11 m. The range of these measurements is independent of the truck speed, but it is affected by scattering of the measurements.

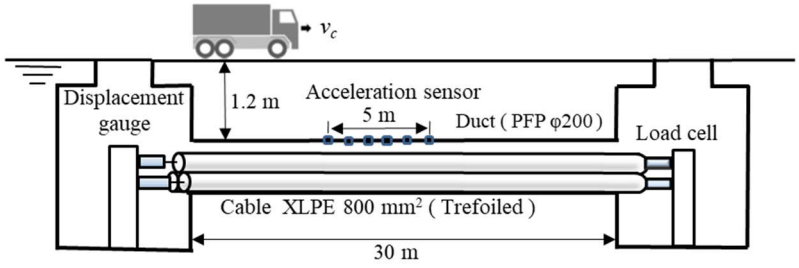

Fig. 11. Overview of the full-scale experiment.

Table I. Experiment conditions

Duct, Cable, Car	PFP φ200; depth d = 1.2 m; single-core cable XLPE 800 mm^2 (W = 108.8 N/m, Young's modulus E = 10); trefoil within a duct; cable (duct) length; L = 30 m; car weight w_c = 20 tf; velocity v_c = 20, 30, 40 km/h			
Road	Course	Thickness mm	Young's modulus MPa	Poisson's ratio
	Surface	50	4000	0.35
	Binder	50	800	0.35
	Base	Lower	800	0.40
Duct deflection (Measured values)	Vertical displacement: 90–140 μm Longitudinal area length of the deflection: 7–11 m			

3.2 Experimentally obtained and analytically obtained results

Figs. 4 and 5 present FEM analysis results obtained for ground displacement under the full-scale experiment conditions. Fig. 4 shows that the vertical displacement of the ground is 90 μm, which shows good agreement with the measured results. The longitudinal displacement of the duct deflection under this condition is 16 μm, as shown in Fig. 5. Fig. 12 presents a comparison between the experimentally obtained results and the analytically obtained results under the experiment conditions. The round and square symbols represent experimentally obtained values. Solid and dashed lines respectively show analytically obtained values representing the lower and upper phase cables. Under the analysis conditions, the weights of the

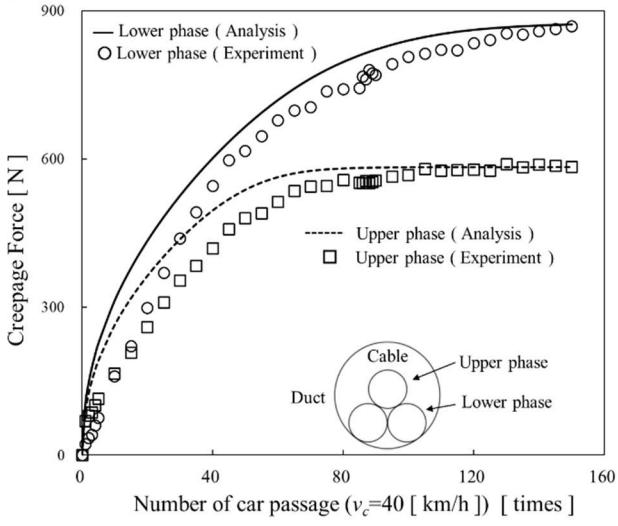

Fig. 12. Experimentally obtained and analytically obtained values of cable creepage force.

two lower-phase cables were set to 1.5 times each, assuming that the weight of the upper-phase cable is applied equally to the two lower-phase cables. The dynamic friction coefficient between the duct and the cable was set as μ_d = 0.27. The dynamic friction force acting on the upper-phase cable with the lower-phase cable sheath was set as μ_d = 0.25, which is smaller than the dynamic friction force with the duct. The analytically obtained values agreed well with the experimentally obtained values, confirming the validity of the theory developed for this study. The cable creepage force tends to saturate at about 900 N for the lower phase cable and at about 550 N for the upper phase cable. Such saturation characteristics of the cable creepage force were reported in experimentally obtained results [3].

4. CONDITIONS OF CABLE CREEPAGE OCCURRENCE

Soft ground and shallow duct burial depths have been reported as conditions exhibiting a strong tendency to cause cable creepage. Single-core cables are more prone to cable creepage than triplex cables. As explained in this chapter, cable creepage movement was analyzed for different conditions under general facility conditions in Japan. Their conditions of occurrence are discussed.

4.1 Analysis conditions

Table II shows the analysis conditions for the duct and car. Although cable creepage increases with the amount of longitudinal displacement of the duct, in this chapter, to clarify the conditions of cable creepage occurrence, the maximum longitudinal displacement of the duct was set as constant at 35.7 μm at each depth by changing the car weight. Duct length of 300 m is a common condition for actual installations in Japan. The car speed was set as v_c =40 km/h. Fig. 13 portrays the longitudinal distribution of the longitudinal component of the ground (duct) displacement. In this displacement area, static friction force acts on the cable placed in the duct. The cable analysis conditions are shown in Table III. Cables of two types with different Young's modulus E used in actual facilities were subjected to analyses.

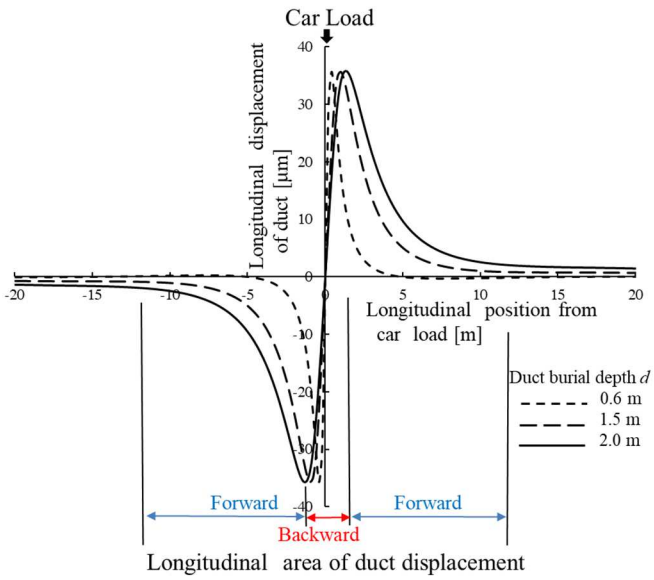

Fig. 13. Longitudinal distribution of longitudinal component of ground (duct) displacement.

Table II. Analysis conditions for ducts and cars

Item		Setting value		
Duct burial depth d	m	0.6	1.5	2.0
Car weight w_c	tf	8.57	20	27.17
Maximum longitudinal duct displacement	μm	35.7		
Duct length L	m	300		

Table III. Analysis conditions for cables

Items \ Cable type		Single-core (XLPE 800 mm^2)	Triplex (XLPE 150 mm^2)
Weight W	N/m	108.8	112.7
Longitudinal elasticity $EA \times 10^6$	N	8.01 (Young's modulus E = 10)	1.47 (E = 3.3)
Dynamic friction coefficient μ_d		0.3, 0.4, 0.5	0.3, 0.4

4.2 Overview of Analysis Results

Figs. 14 and 15 respectively depict the longitudinal distribution of the cable creepage force (cable internal stress) and elongation for the single-core cable. The duct burial depth d was 1.5 m. The dynamic friction coefficient μ_d was 0.4. The origin is the side where the car enters (upstream end). The cable end

at this point is the constrained condition. Point 300 m is the side where the car leaves (downstream end). The cable end is the released condition. The creepage forces presented in Fig. 15 are tensile stress for positive values and compressive stress for negative values. The maximum value of the creepage force is 8.63 kN at the upstream end. Fig. 15 presents the maximum elastic elongation of the cable as 159.7 mm at the 300 m point of the release end.

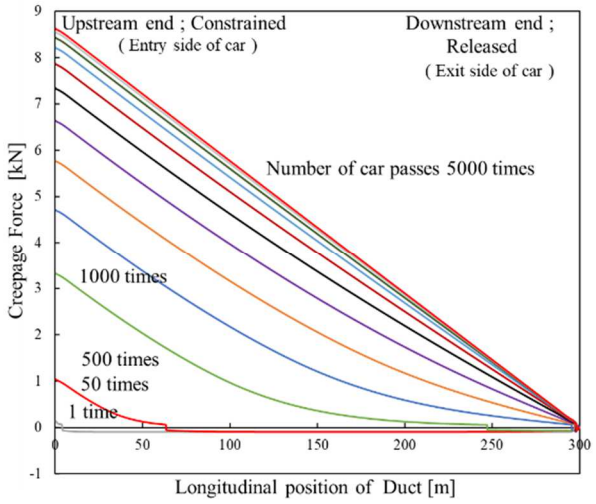

Fig. 14. Longitudinal distribution of cable creepage force (single-core, d = 1.5 m, μ_d = 0.4).

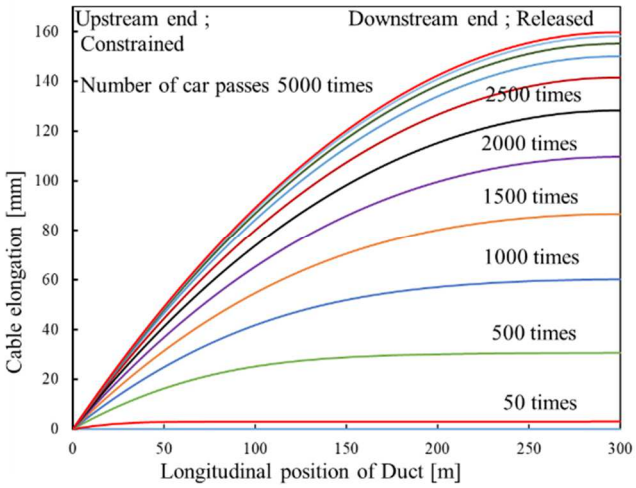

Fig.15. Longitudinal distribution of cable elongation (single-core, d = 1.5 m, μ_d = 0.4).

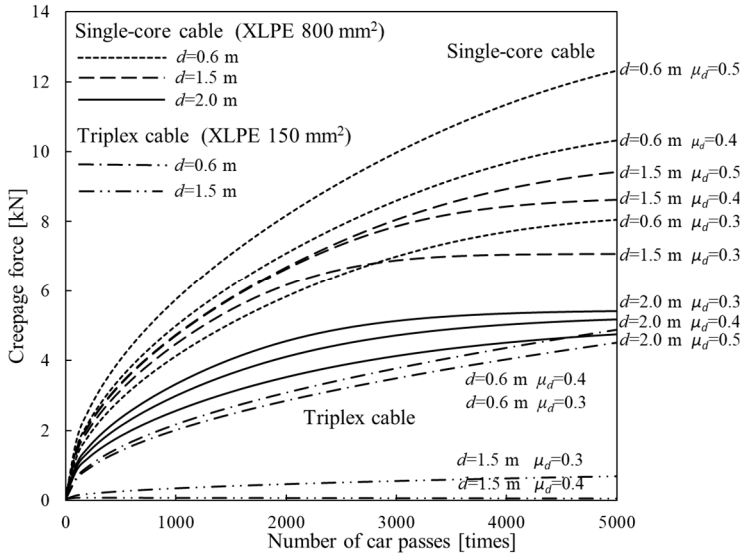

Fig. 16. Variation of the maximum cable creepage force with the number of car passes.

Fig. 16 presents variation of the maximum cable creepage force with the number of car passes for the analysis conditions shown in Tables II and III. The cable creepage force increases under the condition of the single-core cable with large longitudinal elasticity and the shallow duct burial depth. The saturation characteristics are also shown.

4.3 Cable creepage force magnitude and saturation characteristics

Reasons underpinning the saturation characteristics of the cable creepage force are presented in Fig. 16, which depicts a focused view of the analysis results in Fig. 14 from one to five car passes. In this figure, the internal stress in the cable at the first pass of the car is tensile force near the upstream end. It changes to compressive force at about 4 m downstream. The frictional force, which is dominant in the forward area, acts on the cable, causing tensile stress near the constrained upstream end and causing elastic elongation of the cable. This elastic elongation of the cable is held by the static frictional force with the duct in this area such that tensile stress remains in the cable. As the number of car passes increases, the

area of tensile stresses increases in the downstream direction. The static frictional forces that hold the cable elongation increase. Therefore, the cable tensile stress accumulates. After the area of tensile stress reaches the downstream end, the accumulation of cable tensile stress slows and reaches a steady state because no further increase of static frictional force occurs to hold the elastic elongation of the cable. For a deeper duct d = 2.0 m, the accumulated cable tensile stress decreases because the length of the tensile stress area per car passage increases, thereby decreasing the number of car passages until the steady state is reached.

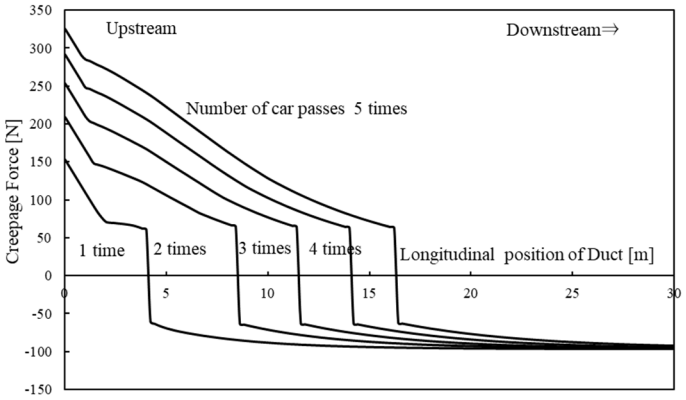

Fig. 17. Accumulation of cable creepage force (number of car passes: 1–5 times).

4.4 Occurrence Conditions of Cable Creepage

Fig. 15 shows the analysis results for the same amount of longitudinal displacement of the duct for each depth. Based on the relation between the cable elastic displacement ΔC_l and the longitudinal displacement of the duct ΔD_l attributable to the static friction force described in Figs. 9 and 10, the conditions for the occurrence of cable creepage force can be classified as shown in Table IV. Under condition (2), as μ_d increases, the return of the cable in the backward area becomes larger and the creepage force decreases.

Table IV. Occurrence conditions of cable creepage

	Equipment conditions	Creepage force	Length of ΔC_l and ΔD_l
(1)	Single-core cable d = 0.6, 1.5 m	Increase at μ_d increase	Both forward and backward area: $\Delta C_l < \Delta D_l$
(2)	Single-core cable d = 2.0 m	Decreases at μ_d increase	forward area: $\Delta C_l \approx \Delta D$ backward area: $\Delta C_l < \Delta D$
(3)	Triplex cable d = 1.5 m	Almost zero at μ_d = 0.4	Both forward and backward area: $\Delta C_l \approx \Delta D_l$

d duct depth, μ_d dynamic coefficient

5. MEASURES AGAINST CABLE CREEPAGE

5.1 Measures to be taken when planning facilities

The most effective countermeasure is to reduce the amount of longitudinal displacement of the duct because of car loads. To achieve this reduction, the following methods should be considered: laying the duct in hard ground, selecting backfill material, and increasing the duct burial depth. Then, in the relation between the longitudinal displacement area length of the duct and the cable longitudinal elasticity, conditions of cable creepage occurrence are classifiable as shown in Table IV. The facility plan is expected to have the conditions presented in Table IV.(3). Even if this condition is difficult to meet, condition (2) must at least be satisfied because the frictional force usually increases with time after the cable was laid in the duct. Using the cable creepage analysis system, one can ascertain these conditions quantitatively.

5.2 Measures for existing facilities

A common countermeasure against cable creepage in existing facilities is to restrain the upstream end of the cable in an access port. However, in situations with strong cable creepage forces, restraining the cable at a single location might damage the restrained parts of the cable or might require widening of access ports to provide space for installing numerous restraining cleats. In such cases, measures to spring

restrain both the upstream and downstream ends of the cable can be considered. Restraining the downstream end of the cable might cause the cable to buckle if excessive compressive force is applied, but by using the cable creepage analysis system to calculate the internal stress of the cable quantitatively, one can design the cable to avoid buckling.

6. CONCLUSION

The authors reported that the cable creepage phenomenon results from the local longitudinal displacement of the duct attributable to the car load. This finding is attributable to the following mechanism.

(1) The car load causes localized deflection of the ducts in the ground. This deflection has a horizontal (longitudinal) displacement component. This longitudinal displacement of the duct causes a static frictional force to act on the cable, resulting in elastic displacement of the cable.

(2) Under conditions where the elastic displacement of the cable is smaller than the longitudinal displacement of the duct, a displacement difference occurs between those. As the car moves longitudinally over the duct, the displacement difference also moves at the same speed, local longitudinal sliding velocities are generated between the duct and cable. These sliding velocities consist of a forward area in the direction of the car's motion and a backward area in the opposite direction.

(3) The Amonton–Coulomb friction law states that the dynamic friction force is independent of the sliding speed. Applying the Amonton–Coulomb friction law to the sliding velocities between the duct and cable shows that the amount of dynamic friction force acting on the cable is greater in the forward area than in the backward area, as presented below. This difference in the dynamic friction force amounts causes the cable to move in the forward direction.

Absolute value of maximum dynamic frictional force	: (Forward) = (Backward)
Area length of dynamic frictional force	: (Forward) > (Backward)
(Absolute value) × (Area length)	: (Forward) − (Backward) > 0

Based on this theory, we developed a cable creepage analysis system that is readily useful on an ordinary PC for cable design and maintenance. Furthermore, the theory validity was verified by conducting a full-scale experiment and by confirming that the measured and analyzed values showed good agreement. Using the developed cable creepage analysis system, one can quantitatively elucidate the conditions under which cable creepage does not occur and can prepare practical countermeasures such as spring restraints at both ends of the cable.

BIBLIOGRAPHY

[1] Electric Technology Research Association. “The present and future engineering technology applied for XLPE cables installation,” (Vol. 61-1. Japan, November 2005. (in Japanese))

[2] A.C. Timmis. “The Creepage of Underground Cable” (POEEJ, Vol. 30, 1937, pp. 180-185)

[3] Y. Watanabe, K. Kanazawa, T. Sasaki. “Measures Against Creepage of 275 kV HPFF Cable” (IEEE Transactions on Power Delivery, Vol. 4, No. 1, 1989, pp. 25-33)

[4] J.K. Kim, J.S. Yi. “Kinematics of Cable Creepage,” (IEEE Transactions on Power Delivery, Vol. 14, No. 1, 1999, pp.1-7)

[5] V.L. Popov, “Contact Mechanics and Friction: Physical Principles and Applications” (Springer, April 2010)

[6] T. Kamibayashi et al. “Development of Analytical Method for Cable Creepage Phenomenon in Duct” (IEEJ Transactions on Power and Energy, Vol. 140, No. 4, 2020, pp. 277-285. (in Japanese))

[7] K.L. Johnson. “Contact mechanics” (Cambridge University Press, Ninth printing 2003)

[8] T. Kamibayashi et al. “A Study of the Power Cable Creepage in the Duct (No. 6)” (2018 National Convention Record, IEEJ Japan, No. 7-127, Japan, 2018, pp. 198-199. (in Japanese))